

Tetragonal and Orthorhombic Phases in Polycrystalline $\text{Sr}_4\text{Ir}_3\text{O}_{10}$ Synthesized by High-Pressure and High-Temperature Technique

Huaxiang Wang, Dabiao Lu, Weipeng Wang, Yifan Ding, Yu Ji, Xi Shen,* Yuan Yao, Youwen Long, and Richeng Yu*

The macroscopic physical properties of materials are determined by their crystal and electronic structures. Iridates have anomalous electronic structures because of the competition of comparable energies between the Coulomb repulsion of electrons and spin-orbit coupling. The polycrystalline $\text{Sr}_4\text{Ir}_3\text{O}_{10}$ sample is successfully synthesized, which owns a trilayered perovskite structure using the high-pressure and high-temperature technique. The transmission electron microscopy studies give the structural evidence of $\text{Sr}_4\text{Ir}_3\text{O}_{10}$ in real space experimentally. It is proved that tetragonal and orthorhombic structures with $I4/mmm$ and $Pbca$ space groups coexist in the polycrystalline $\text{Sr}_4\text{Ir}_3\text{O}_{10}$ sample.

Strontium iridium oxides $\text{Sr}_{n+1}\text{Ir}_n\text{O}_{3n+1}$ ($n = 1, 2, 3, \infty$) belong to Ruddlesden-Popper (RP) perovskite compounds in which the Ir ion has five electrons in the $5d$ orbital. The Ir atom is at the center of an octahedral space made up of the surrounding O atoms. Degenerate $5d$ orbitals of Ir ion split into t_{2g} band with lower energy and e.g., band with higher energy, which is driven by the octahedral symmetric crystal field.^[6] The traditional Hubbard model suggests that iridium oxides with odd electrons in the outmost orbitals should be more metallic than $3d$ and $4f$ element materials because $5d$ orbitals are more extended in space,^[7] which increases the electronic bandwidth and weakens the interaction between electrons of $5d$ orbitals. However, both Sr_2IrO_4 and $\text{Sr}_3\text{Ir}_2\text{O}_7$ have been experimentally found as exotic insulators.^[8,9]

1. Introduction

Transition metal oxides (TMOs), as unique compounds, have always been a hotspot because of their scientific research value and wide industrial application. It is due to the strong electron correlation in TMOs that results in an extremely fruitful field of physical phenomena such as spintronics, multiferroicity, and high- T_c superconductivity.^[1–3] These materials with surprising or even revolutionary physical properties are worth studying. The interest has been focused on $3d$ elements TMOs for several decades. The partial corresponding heavier $4d$ and $5d$ elements are paid less attention because of a small quantity of their compounds and high production cost. For example, $4d$ and $5d$ TMOs, represented by Ru and Ir oxides,^[4,5] exhibit particular competitions among several fundamental interactions which cause novel physical features apparently differing from their $3d$ counterparts.

To resolve the contradiction between conventional band theory and experiments and elucidate the abnormal physical phenomena in $5d$ electron iridium oxides, a novel $J_{\text{eff}} = 1/2$ Mott state induced by a combination of relativistic spin-orbit coupling (SOC) and on-site Coulomb repulsion U was proposed.^[10] Markedly, SOC is not considered in the Hubbard model, it is a relativistic effect.^[11] SOC is about 0.4 eV in iridates and U is ≈ 0.4 –2 eV, which means that SOC in iridates is comparable in energy with U .^[12] The SOC is so strong to split the t_{2g} band into $J_{\text{eff}} = 1/2$ and $J_{\text{eff}} = 3/2$ states. The $J_{\text{eff}} = 3/2$ states can accommodate four $5d$ electrons, and one electron is left to occupy partially the $J_{\text{eff}} = 1/2$ band near the Fermi level. Furthermore, the strong SOC along with U opens a gap in $J_{\text{eff}} = 1/2$ band to produce the Mott insulating state iridates.^[10]

In recent years, a lot of intriguing phenomena have been found in iridium compounds.^[13–16] It is particularly obvious that iridium oxides may become important materials because of the delicate interaction among SOC, U , and other competing couplings, which offers a variety of possibilities for discovering new physics and developing new devices. Sr_2IrO_4 and $\text{Sr}_3\text{Ir}_2\text{O}_7$, which are typical RP perovskite iridium compounds, have been widely investigated.^[8–10] Nonetheless, the same series RP perovskite compound $\text{Sr}_4\text{Ir}_3\text{O}_{10}$ is seldom investigated. Although $\text{Sr}_4\text{Ir}_3\text{O}_{10}$ was reported to be synthesized,^[17] no direct experimental evidence has been presented. In this work, we have successfully synthesized polycrystalline $\text{Sr}_4\text{Ir}_3\text{O}_{10}$ utilizing the high-pressure and high-temperature (HPHT) technique and

H. Wang, D. Lu, W. Wang, Y. Ding, Y. Ji, X. Shen, Y. Yao, Y. Long, R. Yu
Beijing National Laboratory of Condensed Matter Physics
Institute of Physics

Chinese Academy of Sciences

Beijing 100190, P. R. China

E-mail: xshen@iphy.ac.cn; rcyu@iphy.ac.cn

H. Wang, D. Lu, Y. Ding, Y. Ji, Y. Long, R. Yu

School of Physical Sciences


University of Chinese Academy of Sciences

Beijing 100049, P. R. China

R. Yu

Songshan Lake Materials Laboratory

Dongguan, Guangdong 523808, P. R. China

 The ORCID identification number(s) for the author(s) of this article can be found under <https://doi.org/10.1002/pssb.202300050>.

DOI: 10.1002/pssb.202300050

studied its crystal structure using transmission electron microscopy (TEM).

2. Results and Discussion

$\text{Sr}_4\text{Ir}_3\text{O}_{10}$ is reported to be a tetragonal structure ($a = 3.93 \text{ \AA}$, $c = 28.4 \text{ \AA}$) with space group $I4/mmm$ (No. 139),^[17] as shown in **Figure 1a**. This composition is a part of RP structures $\text{Sr}_{n+1}\text{Ir}_n\text{O}_{3n+1}$ with $n = 3$. Here n represents the number of connected SrIrO_3 perovskite layers separated by extra SrO layers. In a unit cell, two groups of triple IrO_6 octahedra arrange along the crystallographic c axis and displace the $a/2$ and $b/2$ directions each other. **Figure 1b** presents the X-ray diffraction (XRD) pattern of the polycrystalline sample where high-intensity peaks are indexed. The XRD pattern indicates that $\text{Sr}_4\text{Ir}_3\text{O}_{10}$ is the main phase with a small quantity of $\text{Sr}_3\text{Ir}_2\text{O}_7$ and SrIrO_3 .

Kafalas et al. reported that $\text{Sr}_4\text{Ir}_3\text{O}_{10}$, $\text{Sr}_3\text{Ir}_2\text{O}_7$, and SrIrO_3 all can be synthesized by the HPHT approach.^[17] The pressures required in synthesizing $\text{Sr}_3\text{Ir}_2\text{O}_7$, $\text{Sr}_4\text{Ir}_3\text{O}_{10}$, and SrIrO_3 are 1, 3.5, and 4.5 GPa, respectively. In view of this, we altered pressure, temperature, and pressure-holding time in the synthesis in a range of 3.5–4.5 GPa, 1073–1273 K, and 0.5–2 h, respectively. Unfortunately, the coexistence of $\text{Sr}_4\text{Ir}_3\text{O}_{10}$, $\text{Sr}_3\text{Ir}_2\text{O}_7$, and SrIrO_3 phases was always detected in XRD patterns. It may be caused by similar free energies of the three phases. Our synthesis experiences indicate the difficulty of synthesizing the pure $\text{Sr}_4\text{Ir}_3\text{O}_{10}$ phase. This may be the reason for the lack of research on $\text{Sr}_4\text{Ir}_3\text{O}_{10}$.

The scanning electron microscopy (SEM) image in **Figure 1c** shows that the polycrystalline grain size is more than several

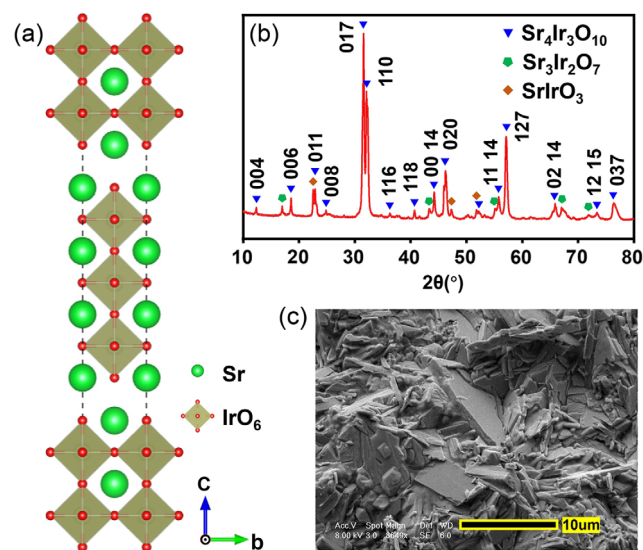


Figure 1. a) The sketch of the crystal structure of $\text{Sr}_4\text{Ir}_3\text{O}_{10}$ with space group $I4/mmm$.^[19] Green spheres and yellow octahedra indicate Sr atoms and IrO_6 octahedra, respectively. Ir atom is at the center and O atoms are at the corner of an octahedron. b) XRD pattern of the polycrystalline sample. Three phases of $\text{Sr}_4\text{Ir}_3\text{O}_{10}$, $\text{Sr}_3\text{Ir}_2\text{O}_7$, and SrIrO_3 are indicated by blue, green, and brown symbols, respectively. The peaks of $\text{Sr}_4\text{Ir}_3\text{O}_{10}$ are indexed by a tetragonal structure. c) An SEM image of the polycrystalline sample.

micrometers. The experimental selected-area electron diffraction (SAED) patterns along the $[001]$, $[100]$, and $[110]$ directions, respectively, are presented in the right panels of **Figure 2a,b**. These SAED patterns can be indexed to a tetragonal structure, consistent with the previous results.^[17] In addition, we simulated SAED patterns in the left panels of **Figures 2a,b** using a landyne software,^[18] and the results agree well with the experimental patterns, also proving the tetragonal $\text{Sr}_4\text{Ir}_3\text{O}_{10}$ phase in the sample. The corresponding high-resolution electron microscopy (HREM) images are presented in **Figure 2c,d**. The enlarged partial images are superimposed at the top right of each HREM image. The HREM images clearly show the characteristics of $\text{Sr}_4\text{Ir}_3\text{O}_{10}$, an RP configuration with $n = 3$. Although tetragonal $\text{Sr}_4\text{Ir}_3\text{O}_{10}$ was reported, we observe structural information directly in real space.

In addition, an orthorhombic $\text{Sr}_4\text{Ir}_3\text{O}_{10}$ phase is also detected in the sample. The sketches of Ir–O octahedra of tetragonal and orthorhombic $\text{Sr}_4\text{Ir}_3\text{O}_{10}$ are shown in **Figure 3**. Compared with the tetragonal structure, the Ir–O octahedra rotate several degrees around the c axis and the in-plane Ir–O–Ir bond is no longer 180° in the orthorhombic structure. Besides, we referred to the out-of-phase structure of $\text{Sr}_3\text{Ir}_2\text{O}_7$.^[9] Ir–O octahedra of adjacent layers rotate in the opposite direction around the same axis. And then the correlation of the basis vectors of the two structures can be described:

$$a_{\text{O}} = a_{\text{T}} + b_{\text{T}} \quad (1)$$

$$b_{\text{O}} = b_{\text{T}} - a_{\text{T}} \quad (2)$$

$$c_{\text{O}} = c_{\text{T}} \quad (3)$$

where a , b , and c are the lattice unit vectors, and the subscripts “O” and “T” denote the orthorhombic and tetragonal structures,

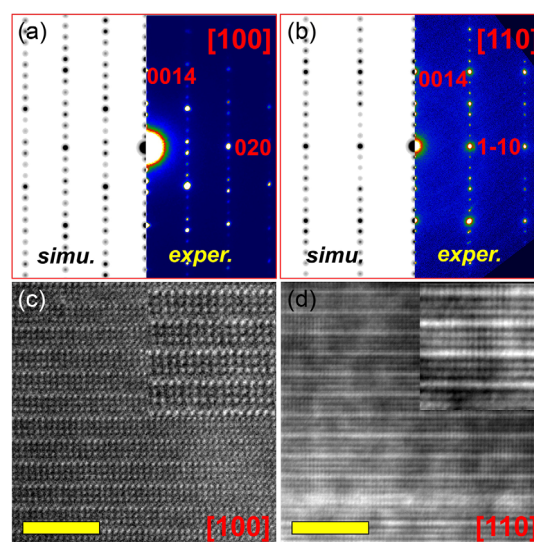


Figure 2. a,b) TEM results of $\text{Sr}_4\text{Ir}_3\text{O}_{10}$. The SAED patterns of $\text{Sr}_4\text{Ir}_3\text{O}_{10}$ along the $[100]$ and $[110]$ zone axes, respectively. The left and right parts of each pattern are the simulated and experimental results, respectively. These diffraction spots are indexed to a tetragonal structure. c,d) The corresponding HREM images of $\text{Sr}_4\text{Ir}_3\text{O}_{10}$. The upper right corner of each image is the enlarged partial image. The yellow scale bar is 5 nm.

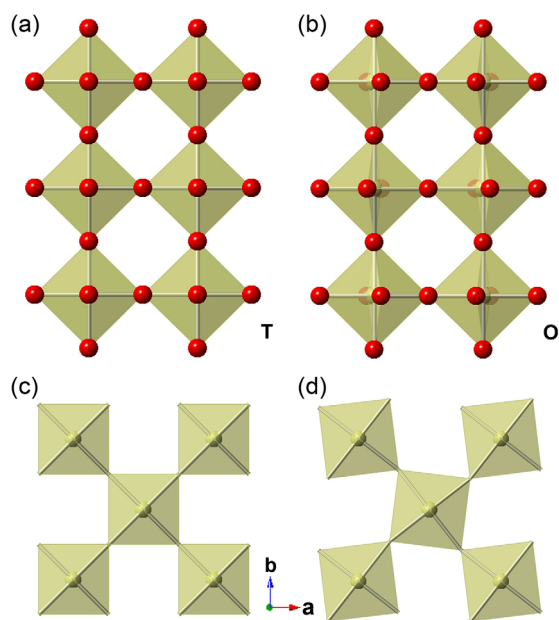


Figure 3. Tetragonal and orthorhombic crystal structures of $\text{Sr}_4\text{Ir}_3\text{O}_{10}$. a) The half-unit cell of $\text{Sr}_4\text{Ir}_3\text{O}_{10}$ with tetragonal symmetry. b) The half-unit cell of $\text{Sr}_4\text{Ir}_3\text{O}_{10}$ with orthorhombic symmetry. Red spheres and yellow octahedra indicate O atoms and IrO_6 octahedra, respectively. Sr atoms are hidden. c) IrO_6 octahedra without rotation perpendicular to the c axis in the tetragonal $\text{Sr}_4\text{Ir}_3\text{O}_{10}$. d) IrO_6 octahedra of one layer in (b) with rotation perpendicular to the c axis in the orthorhombic $\text{Sr}_4\text{Ir}_3\text{O}_{10}$.

respectively. The different characteristics between the two structures can be reflected in their SAED patterns.

According to structures and their rotational octahedron of RP perovskite compounds, we simulated diffraction patterns along the different axes with several structures. One structure with a $Pbca$ space group is consistent with our experimental results. **Figure 4a** shows the simulated and experimental SAED patterns of the orthorhombic $\text{Sr}_4\text{Ir}_3\text{O}_{10}$ along the $[001]$ direction. We attribute the weak reflections of $h = 2n + 1$ in the experimental result to multiple reflections, which correspond to square symbols in the simulated pattern in **Figure 4a**. The diffraction spot pointed by the red arrow indicates the (100) index of the orthorhombic $\text{Sr}_4\text{Ir}_3\text{O}_{10}$, which corresponds to the $\frac{1}{2} \frac{1}{2} 0$ index in the tetragonal structure. Moreover, the experimental SAED pattern along the $[210]_O$ axis of the orthorhombic $\text{Sr}_4\text{Ir}_3\text{O}_{10}$ is presented in **Figure 4b**. The simulated patterns along the $[130]_T$ axis of the tetragonal and the $[210]_O$ axis of the orthorhombic $\text{Sr}_4\text{Ir}_3\text{O}_{10}$ are displayed in **Figure 4b,c**, respectively, for comparison. An obvious difference in the SAED patterns can be seen between the tetragonal and orthorhombic structures of $\text{Sr}_4\text{Ir}_3\text{O}_{10}$, which are indicated by the red arrows in **Figure 4b**. Miller indices with $h = -2$ & $k = 1$ in the orthorhombic structure are absent in the tetragonal structure. These experimental and simulated SAED patterns confirm that there exists an orthorhombic structure of $\text{Sr}_4\text{Ir}_3\text{O}_{10}$ in our sample. The tetragonal and orthorhombic phases of $\text{Sr}_4\text{Ir}_3\text{O}_{10}$ have very similar crystal structures with approximate free energies. There are also closing conditions

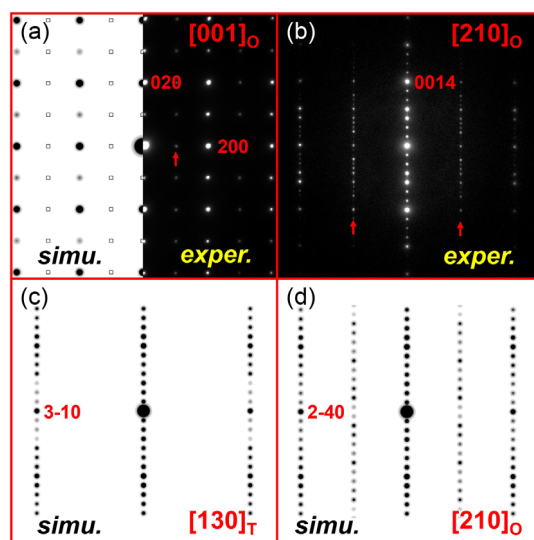


Figure 4. Experimental and simulated SAED patterns of the orthorhombic $\text{Sr}_4\text{Ir}_3\text{O}_{10}$. a) The SAED pattern of the orthorhombic $\text{Sr}_4\text{Ir}_3\text{O}_{10}$ along the $[001]_O$ axis. Simulated and experimental results are displayed in the left and right panels, respectively. The diffraction spots pointed by red arrows represent the absent spots in the tetragonal structure of $\text{Sr}_4\text{Ir}_3\text{O}_{10}$. b) The experimental SAED pattern of the orthorhombic $\text{Sr}_4\text{Ir}_3\text{O}_{10}$ along the $[210]_O$ axis. The diffraction spots signed by red arrows reflect the characteristic information of the orthorhombic structure. c) The simulated SAED pattern of the tetragonal structure of $\text{Sr}_4\text{Ir}_3\text{O}_{10}$ along the $[130]_T$ axis. d) The simulated SAED pattern of the orthorhombic structure of $\text{Sr}_4\text{Ir}_3\text{O}_{10}$ along the $[210]_O$ axis.

for sample synthesis. In the process of sample synthesis, the fluctuation of conditions causes both phases to exist.

3. Conclusion

We have successfully synthesized polycrystalline $\text{Sr}_4\text{Ir}_3\text{O}_{10}$ using the HPHT approach. A tetragonal phase and an orthorhombic phase are confirmed to coexist in the sample. The coexistence of the two phases indicates that the two structures of $\text{Sr}_4\text{Ir}_3\text{O}_{10}$ may have nearly similar free energies.

4. Experimental Section

Polycrystalline $\text{Sr}_4\text{Ir}_3\text{O}_{10}$ was synthesized by the HPHT technique. Sr_2IrO_4 was prepared first from stoichiometric SrCO_3 and IrO_2 powders through a solid-state reaction sintered at 1273 K for 48 h in the atmosphere. Next, Sr_2IrO_4 and IrO_2 were mixed uniformly with a nominal composition of $\text{Sr}_4\text{Ir}_3\text{O}_{10}$ and packed into a cylindrical platinum capsule. Then, a pressure of 3.5 GPa was adopted to press the powders using a cubic-anvil-type high-pressure apparatus at room temperature. Finally, the temperature was heated up to 1073 K and normalized to room temperature after holding constant for 2 h.

The morphology of the sample was characterized by a scanning electron microscope (XL30 S-FEG, FEI). The phase purity of the specimen was examined by XRD equipment (Cu $K\alpha$ radiation, X' Pert Pro MPD, Philips). Thin specimens for TEM were prepared by focused ion beam (Helios 6001, FEI) technique or milling the powders of $\text{Sr}_4\text{Ir}_3\text{O}_{10}$ in an agate mortar and dispersing them in an amorphous carbon film supported by a copper mesh with alcohol. The TEM experiments were performed on transmission electron microscopes (CM200 Philips and JEM 2100Plus) operated at 200 kV.

Acknowledgements

This work was supported by the National Key Research Program of China (grant nos. 2022YFA1402801 and 2018YFA0208402), the National Natural Science Foundation of China (grant nos. 11874413, 11934017, and 51972333), and the Strategic Priority Research Program of the Chinese Academy of Sciences (grant no. XDB33030200). One of the authors, X. S., was sponsored by the Youth Innovation Promotion Association of CAS (2019009).

Conflict of Interest

The authors declare no conflict of interest.

Data Availability Statement

Research data are not shared.

Keywords

high-pressure and high-temperature techniques, $\text{Sr}_4\text{Ir}_3\text{O}_{10}$, tetragonal structures, orthorhombic structures, 5d electron transition metal oxides

Received: February 3, 2023

Revised: May 5, 2023

Published online: May 25, 2023

- [1] S. D. Bader, S. S. P. Parkin, *Annu. Rev. Condens. Matter Phys.* **2010**, 1, 71.

- [2] K. F. Wang, J. M. Liu, Z. F. Ren, *Adv. Phys.* **2009**, 58, 321.
 [3] J. G. Bednorz, K. A. Müller, *Z. Phys. B: Condens. Matter* **1986**, 64, 189.
 [4] Y. Maeno, H. Hashimoto, K. Yoshida, S. Nishizaki, T. Fujita, J. G. Bednorz, F. Lichtenberg, *Nature* **1994**, 372, 532.
 [5] Y. Okada, D. Walkup, H. Lin, C. Dhital, T.-R. Chang, S. Khadka, W. Zhou, H.-T. Jeng, M. Paranjape, A. Bansil, Z. Wang, S. D. Wilson, V. Madhavan, *Nat. Mater.* **2013**, 12, 707.
 [6] Y. Tokura, N. Nagaosa, *Science* **2000**, 288, 462.
 [7] J. Hubbard, *Proc. Roy. Soc. Lond. A: Math. Phys. Sci.* **1963**, 276, 238.
 [8] B. J. Kim, H. Ohsumi, T. Komesu, S. Sakai, T. Morita, H. Takagi, T. Arima, *Science* **2009**, 323, 1329.
 [9] G. Cao, Y. Xin, C. S. Alexander, J. E. Crow, P. Schlottmann, M. K. Crawford, R. L. Harlow, W. Marshall, *Phys. Rev. B* **2002**, 66, 214412.
 [10] B. J. Kim, H. Jin, S. J. Moon, J.-Y. Kim, B.-G. Park, C. S. Leem, Jaejun Yu, T. W. Noh, C. Kim, S.-J. Oh, J.-H. Park, V. Durairaj, G. Cao, E. Rotenberg, *Phys. Rev. Lett.* **2008**, 101, 076402.
 [11] K. V. Shanavas, Z. S. Popović, S. Satpathy, *Phys. Rev. B* **2014**, 90, 165108.
 [12] G. Cao, P. Schlottmann, *Rep. Prog. Phys.* **2018**, 81, 042502.
 [13] G. Jackeli, G. Khaliullin, *Phys. Rev. Lett.* **2009**, 102, 017205.
 [14] J. Chaloupka, G. Jackeli, G. Khaliullin, *Phys. Rev. Lett.* **2010**, 105, 027204.
 [15] F. Wang, T. Senthil, *Phys. Rev. Lett.* **2011**, 106, 136402.
 [16] H. Watanabe, T. Shirakawa, S. Yunoki, *Phys. Rev. Lett.* **2013**, 110, 027002.
 [17] J. A. Kafalas, J. M. Longo, *J. Solid State Chem.* **1972**, 4, 55.
 [18] X. Z. Li, *Microsc. Microanal.* **2016**, 22, 564.
 [19] K. Momma, F. Izumi, *J. Appl. Crystallogr.* **2011**, 44, 1272.